IEEE Photonics Journal
An IEEE Photonics Society Publication

Switchable Dual-Wavelength Synchronously Q-Switched Erbium-Doped Fiber Laser Based on Graphene Saturable Absorber

Volume 4, Number 3, June 2012

Z. T. Wang
Y. Chen
C. J. Zhao
H. Zhang
S. C. Wen

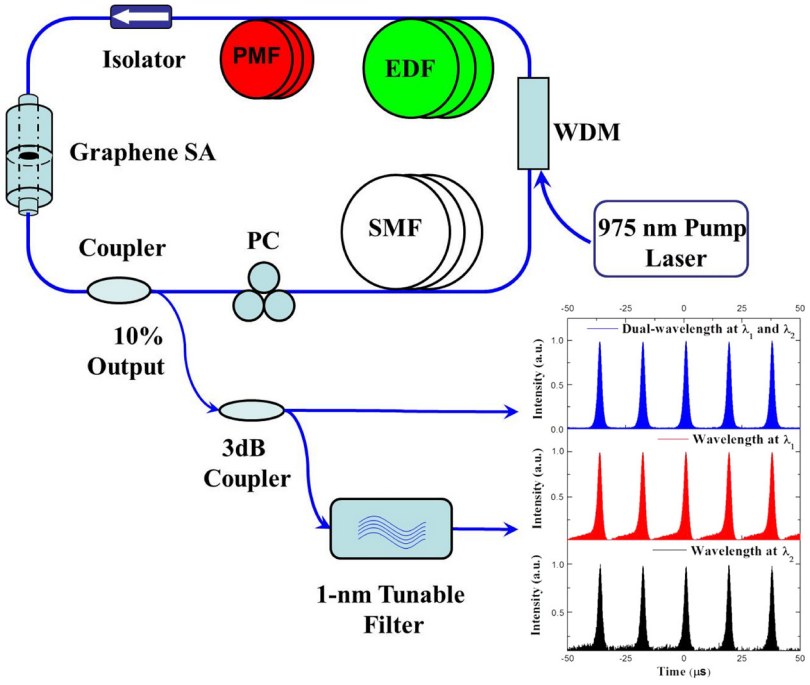

DOI: 10.1109/JPHOT.2012.2199102
1943-0655/$31.00 ©2012 IEEE

Switchable Dual-Wavelength Synchronously Q-Switched Erbium-Doped Fiber Laser Based on Graphene Saturable Absorber

Z. T. Wang, Y. Chen, C. J. Zhao, H. Zhang, and S. C. Wen

Key Laboratory for Micro-/Nano-Optoelectronic Devices of Ministry of Education,
College of Information Science and Engineering, Hunan University, Changsha 410082, China

DOI: 10.1109/JPHOT.2012.2199102

Manuscript received March 30, 2012; revised May 4, 2012; accepted May 5, 2012. Date of publication May 11, 2012; date of current version May 24, 2012. This work was partially supported by the National Basic Research Program (973 Program) of China (Grant 2012CB315701), the National Natural Science Foundation of China (Grant 61025024), the National Natural Science Foundation of China (Grant 61011120106) and Program for New Century Excellent Talents in University (Grant NCET 11-0135). Corresponding author: Z. Wang (e-mail: ztwang1987@163.com).

Abstract: We demonstrate a switchable dual-wavelength synchronously pulsed fiber laser Q-switched by graphene saturable absorber. Wavelength-resolved studies on the output Q-switched pulses show that despite of large wavelength spacing up to 26 nm, the two Q-switched pulses at each individual wavelength can be temporally synchronized with per-pulse energy up to ~70 nJ. Further experiments show that by adjusting the intracavity birefringence, dual-wavelength emission can be switched to another dual-wavelength operation regime with wavelength separation of 5.7 nm. Our experimental results are also qualitatively supported by the cavity linear transmission characteristics of the ring cavity.

Index Terms: Q-switching, fiber laser, graphene, ultrashort pulse.

1. Introduction

Multiwavelength Q-switching lasers show versatile applications in metrology, environmental sensing, microwave optics, biomedical diagnostics, range finding, laser processing, and telecommunications [1]–[3]. Some techniques had been proposed to deliver multiwavelength Q-switched pulse, including active [4] and passive [5]–[11] approaches. Recently, graphene, a 2-D form of carbon material, was developed as a saturable absorber (SA), taking the advantage of its broadband saturable absorption property with ultrafast recovery time of ~200 fs, and a wide operation spectral range covering several micrometers, due to its unique linear energy band structure [12]–[15]. Wavelength tunable pulsed lasers based on graphene SA with the tuning range up to several tens of nanometers have been reported [16]–[18]. Moreover, graphene SA could be used to mode lock Yb- [19], and Er-doped [20] fiber laser operating at the wavelengths of 1.05 μm and 1.56 μm, respectively. However, all the aforementioned contributions belong to the type of single-wavelength operation. More recently, Luo *et al.* reported a dual-wavelength Q-switched fiber laser based on graphene SA, with a wavelength spacing of only 0.2 nm [21]. In this paper, with the help of graphene SA, we are able to generate a train of dual-wavelength Q-switched pulse but with much wider wavelength separation in an erbium-doped fiber (EDF) laser. We also noted that the Q-switched pulses at two individual wavelengths can be synchronized and temporally overlapped. Furthermore, the operation regime can

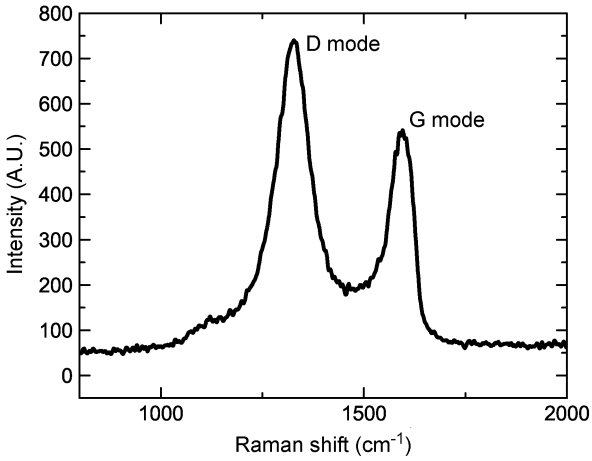

Fig. 1. Raman spectrum of the graphene sample.

be switched to another dual-wavelength Q-switching state peaked at 1555.8 nm and 1561.5 nm with wavelength spacing of 5.7 nm. Based on the cavity linear transmission analysis, we show that the intracavity birefringence-induced comb filtering is dependent on the polarization controllers (PCs) setting and responsible for this type of dual-wavelength emission.

2. Experimental Setup and Graphene SA

The graphene SA is prepared by two steps. First, graphene sample is prepared by chemical reduction of exfoliated graphite oxide (GO) reported by Stankovich *et al.* [22]. GO is mixed with water to yield well-dispersed graphene oxide suspension, then the graphene oxide in the suspension is reduced by hydrazine hydrate/NH_3 to obtain basic graphene suspension. The product is isolated by filtration, washed copiously with water and methanol, and dried on the funnel under a continuous airflow through the solid product cake [22]. Raman spectrums of graphene sample were detected and plotted in Fig. 1. The *G* peak corresponds to the E_{2g} phonon at the Brillouin zone center. The *D* peak is due to the breathing modes of sp^2 rings and requires a defect for its activation by double resonance. The high ratio between the intensity of *G* peak and *D* peak implies the graphene samples have a large amount of structural defects. Secondly, the graphene is transferred and deposited onto a fiber ferrule by the optical deposition method [23]. In order to achieve the graphene dispersion, the graphene suspension is made by mixing 3 mg graphene powder with 10 ml dimethylformamide (DMF) solution. Efficient dispersion is achieved after 30 minutes of ultrasonication. The solutions are then subjected to centrifugation in order to separate the remaining macroscopic flakes of graphene. The visually homogeneous part of the solution is picked up for the optical deposition process. Experimental setup for the optical deposition of graphene on the end facet of fiber ferrule is shown in Fig. 2(a). The incident light with power of 80 mW from a 1480 nm laser diode (LD) is injected from a flat fiber ferrule facet end into the solution. After 3 minutes laser injection, graphene is gradually trapped onto the core of the fiber ferrule due to a combination of optical trapping and heat convention effects [24]. After the optical deposition process, the fiber ferrule is taken away from the solution and then air-dried for several hours. The fiber ferrule with several-layer graphene connects with another new fiber ferrule to form a fiber-compatible graphene SA. Finally, the graphene SA is spliced into a laser cavity as a passive Q-switcher.

Fig. 2(b) shows the experiment setup of graphene-based passively Q-switched switchable dual-wavelength EDF ring laser. A piece of EDF is 3 m with group velocity dispersion 10 (ps/nm)/km at 1550 nm and peak core absorption 16 dB/m at 1530 nm. One segment of 0.5 m polarization maintenance fiber (PMF) with beat length 2.4 mm and group velocity dispersion 15 (ps/nm)/km at 1550 nm is deliberately spliced into the fiber laser cavity so as to ensure that the laser cavity is operated at high birefringence regime. The splicing loss due to PMF is about 0.5 dB. The rest is 50 m long single-mode fiber (SMF) with group velocity dispersion 18 (ps/nm)/km at 1550 nm. A

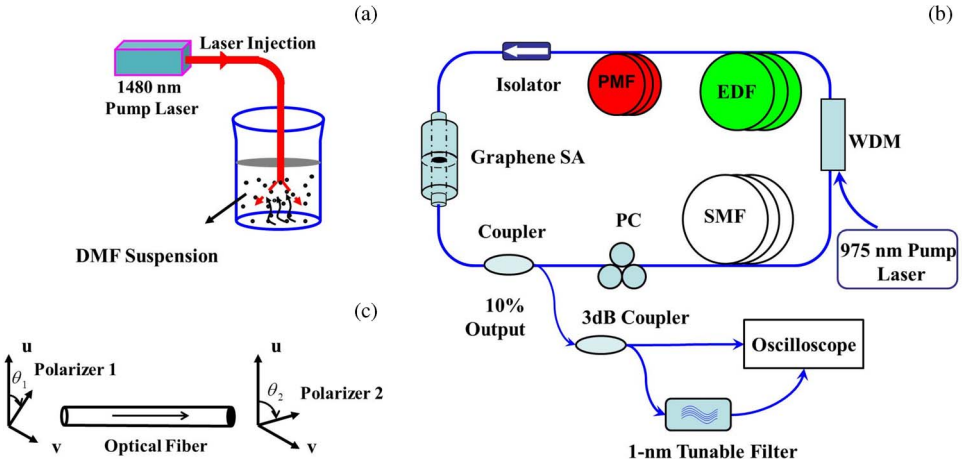

Fig. 2. (a) The optical deposition setup of depositing graphene on the end facet of fiber ferrule. (b) The scheme of the proposed dual-wavelength Q-switched fiber laser. WDM: wavelength division multiplexer. Graphene SA: graphene saturable absorber. PCs: polarization controllers. EDF: erbium-doped fiber. SMF: single-mode fiber. PMF: polarization-maintaining fiber. (c) The simplified setup of cavity transmission. *u* and *v* are the fast and slow axes of the fiber, respectively.

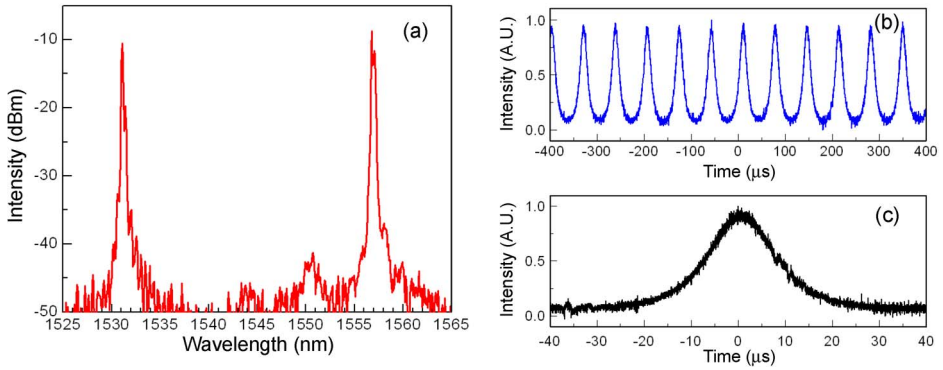

Fig. 3. Dual-wavelength Q-switching operation when pump power is 153.9 mW, (a) the spectrum of the pulse, (b) oscillogram of the obtained pulse train, (c) shape of the individual pulse.

polarization-dependent isolator (PDI) is used as a polarizer and an isolator to ensure unidirectional light propagation. A graphene-SA is used as the Q-switching component. The PC is employed to fine-tune the linear cavity birefringence. The total cavity length is 63.5 m, including several pieces of passive fibers for connecting the components, and the total cavity dispersion is about $-1.45 ps^2$. A 980/1550 nm wavelength-division multiplexer (WDM) is used to launch the pumped light into the laser cavity. A 10% coupler is employed to couple out light. The laser is pumped by a 975 nm ALD98-500-B-FA diode laser. The output light is analyzed by optical spectrum analyzer (AQ-6315A), a 500 MHz oscilloscope (TDS3054B) and a photodetector.

3. Experimental Results and Discussion

Q-switching operation in our fiber laser is achieved by graphene SA. CW state of dual-wavelength operation is obtained at a pump power above 40 mW, corresponding to the laser threshold. The laser can operate on dual-wavelength Q-switching once the pump power exceeds 120 mW. Fig. 3 shows the dual-wavelength Q-switched pulse train at the pump power 153.9 mW. The two simultaneous Q-switching lasing wavelengths center at 1531.12 nm and 1556.79 nm with 3-dB bandwidth 0.18 nm and 0.31 nm, respectively, as shown in Fig. 3(a). The wavelength spacing is

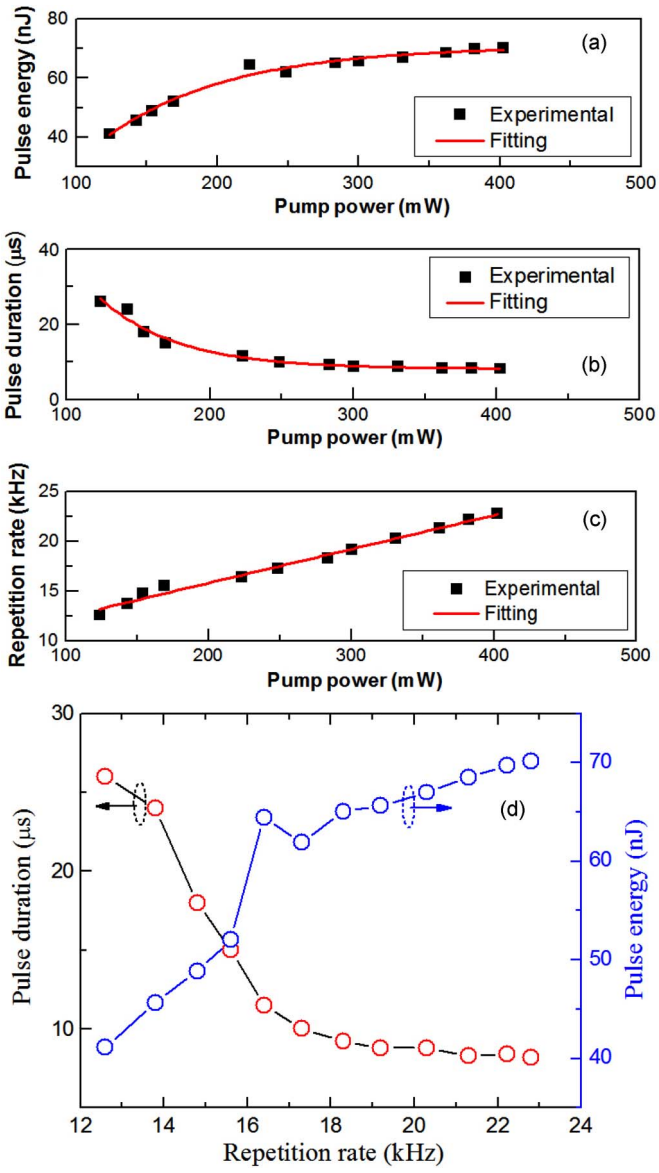

Fig. 4. (a) Single pulse energy, (b) pulse duration, (c) repetition rate versus pump power and (d) the relation between per-pulse energy (pulse duration) and different repetition rate.

25.6 nm. Fig. 3(b) shows the oscilloscope trace of Q-switched pulse. The FWHM of the Q-switching pulse is 18.1 μs. The repetition rate of pulse is 14.9 kHz, corresponding to a pulse interval of 67.1 μs.

To investigate the dynamics of the dual-wavelength pulsed fiber laser, we increase the pump power while keeping the PCs unchanged. As the pump power increases from 123.5 mW to 402.6 mW, the pulse duration decreases from 26.5 μs to 8.2 μs while the repetition rate increases from 12.6 kHz to 22.8 kHz, as shown in Fig. 4. The position and the wavelength separation of the two lasing peak insensitively depend on pump power. The single pulse energy can reach up to 70.2 nJ, ten times larger than the energy of mode-locked pulse [14], [25], by increasing the pump power up to 402.6 mW. Even higher energy pulse is obtainable but limited by the maximum available pump power in our laser. Based on the fitting curve of Fig. 4(b), we assume that the minimum pulse duration in our experiment can reach down to 8.15 μs. Fig. 4(d) shows the relation between per-pulse energy (pulse duration) and different repetition rate.

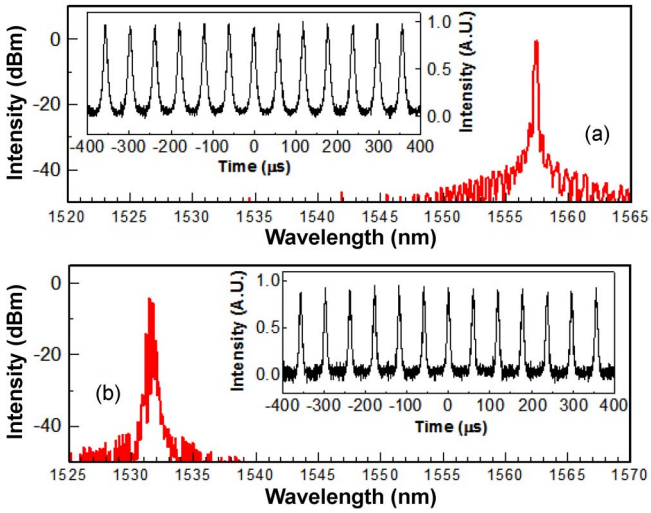

Fig. 5. Spectrum and oscillogram (insert) of pulse train at (a) 1556.79 nm and (b) 1531.12 nm under a pump power of 248.6 mW.

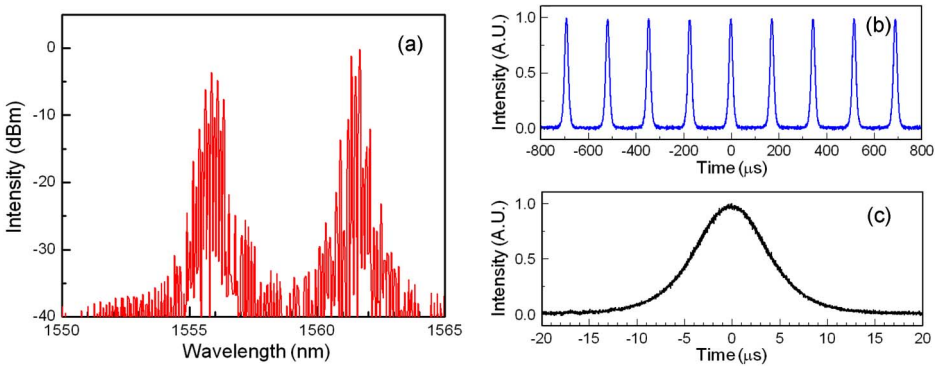

Fig. 6. Another dual-wavelength Q-switching operation after rotating PCs under a pump power of 248.6 mW, (a) spectrum, (b) corresponding oscillogram, (c) corresponding pulse profile.

A 1-nm bandpass tunable optical filter is used to resolve the laser output. Fig. 5 shows the individual pulse train with center wavelength at 1556.79 nm and 1531.12 nm at a pump power of 248.6 mW, respectively. Each pulse train has the same repetition rate of 17.3 kHz, which also corresponds to the repetition rate of the total dual-wavelength Q-switched pulse, as shown in Fig. 4(c). The pulse duration at 1531.12 nm and at 1556.79 nm are 8.8 μs and 9.15 μs, respectively. On the oscilloscope trace, we note that these two individual wavelength components are static and relative movement is not observed, indicating that two sets of Q-switched pulses at different wavelengths are temporally synchronized, despite of large center wavelength difference.

Further rotation of the PCs yields the emission of dual-wavelength Q-switched pulse train with tunable wavelength spacing. Fig. 6 shows the output of the laser at a pump power of 248.6 mW after rotating PCs. In Fig. 6(a), the peak wavelengths are located at 1555.8 nm and 1561.5 nm with wavelength separation of 5.7 nm. The pulse duration is 8.8 μs with repetition rate of 11.6 kHz. By reversely rotating the PCs, the laser can return to another operation regime with wavelength spacing of 25.6 nm. Changing the bias of the PCs, which correlates to the variation of the intracavity fiber birefringence, could lead to the continuous change of the channel spacing and peak position of the birefringence-induced comb filter. Correspondingly, different spectral transmission distribution can be achieved. This can explain why the emission wavelength of dual-wavelength Q-switching pulses can be switchable by adjusting the paddles of PCs.

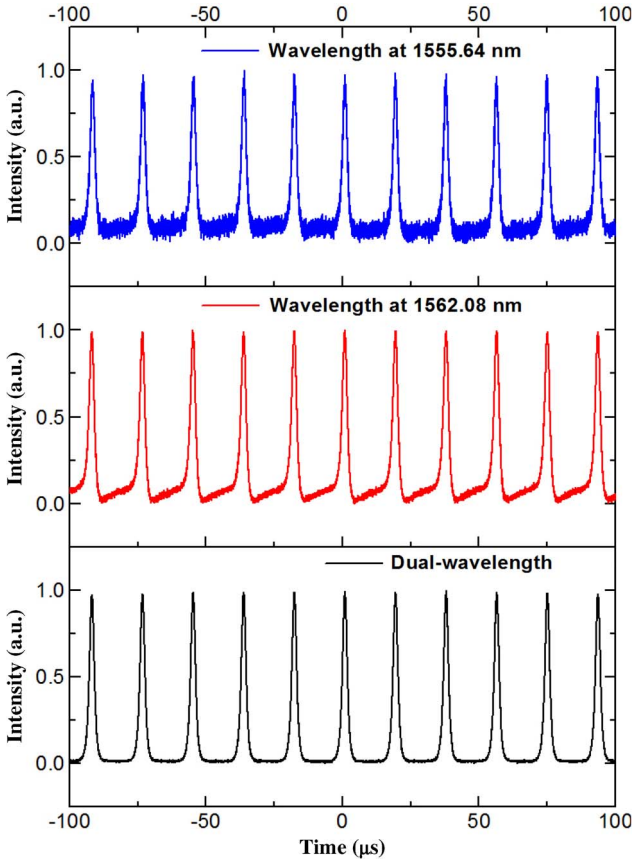

Fig. 7. Wavelength resolved oscilloscope traces of one single wavelength at 1555.64 nm, another single wavelength at 1562.08 nm and dual wavelength at both 1555.64 nm and 1562.08 nm. It shows that there is no obvious time delay between each wavelength.

In order to investigate whether oscilloscope trace of each wavelength shows temporal delay or not, we deliberately perform a comparative experiment as follows. An 50% output coupler is used to resolve the cavity output and one optical route is directly connected with one photodetector in one channel of the oscilloscope while the other optical route is connected with the L-band transmission filter, which is then connected to another photodetector in another channel of the oscilloscope. By changing the transmission filter performance, we can simultaneously monitor the oscilloscope trace at one wavelength and oscilloscope trace at the dual-wavelength. Experimentally, by setting the dual-wavelength Q-switching state as the reference clock, we can record the wavelength resolved oscilloscope traces of one single wavelength at 1555.64 nm, another single wavelength at 1562.08 nm and dual-wavelength at both 1555.64 nm and 1562.08 nm as shown in Fig. 7. By carefully examining the temporal of oscilloscope traces of each wavelength and dual-wavelength, we are able to conclude that there is no obvious temporal delay between each wavelength based on the observed dual-wavelength Q-switching state.

The dual-wavelength and wavelength-switched operations are obtainable without any wavelength selective elements in our experiment due to the birefringence-induced filter effect of the cavity. The PDI, combined with the PMF, acts as an intracavity birefringence-induced comb filter [26]–[29]. The design of our laser cavity can be described as a simple model shown in Fig. 2(c). The cavity transmission is [30]–[32]

$$T = \cos^2\theta_1\cos^2\theta_2 + \sin^2\theta_1\sin^2\theta_2 + \frac{1}{2}\sin(2\theta_1)\sin(2\theta_2)\cos(\Delta\Phi_{PC} + \Delta\Phi_L + \Delta\Phi_{NL}) \quad (1)$$

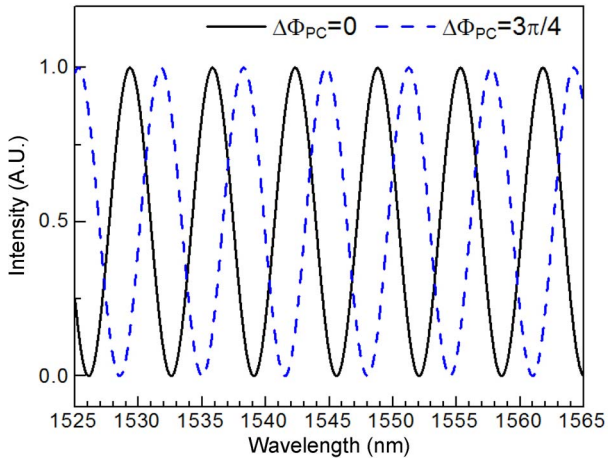

Fig. 8. Calculated transmission spectra at $\Delta\Phi_{PC} = 0$ (black solid line) and $\Delta\Phi_{PC} = 3\pi/4$ (blue dashed line).

where θ_1 and θ_2 are the angles between the polarization directions of the polarizers and the fast axes of the fiber, $\Delta\Phi_L = 2\pi(n_v - n_u)L/\lambda$ and $\Delta\Phi_{NL} = 2PL\gamma\cos 2\theta_1/3$ are the linear and the nonlinear cavity phase delay caused by fiber, respectively. $\Delta\Phi_{PC}$ is the PC-induced phase delay. L is equal to the fiber length, λ is the operating wavelength, γ is the nonlinear coefficient, n_u and n_v are the refractive index of the fast axes and slow axes of the fiber, respectively, and P is the instantaneous power of input signal. The beat length of the PMF and SMF are equal to 2.4 mm and 2 m, respectively. If the power of incident light is assumed to be sufficiently lower, the nonlinear phase shift can be ignored. The transmission coefficient varies periodically with respect to the wavelength, as shown in Fig. 8. It can be considered as a spectral comb filter whose channel separation depends on the intracavity birefringence. Due to the birefringence of the fiber, changing the bias of the PC can lead to different birefringence of the cavity, resulting in the change of the channel spacing and peak position of the birefringence-induced comb filter. Thus different transmission distribution of spectrum can be obtained. It accounts for the emission wavelength of dual-wavelength Q-switching pulses can be switchable by adjusting the PCs.

The laser cavity under investigation is a typical energy conservative system where loss is automatically balanced by the gain, and therefore dual-wavelength emission could be obtained at different pump powers. To understand the operation mechanism of dual-wavelength emission, we also deliberately remove the PMF in order to isolate the laser operation without birefringence-induced comb filtering effect. We find that the dual-wavelength operation is difficult to achieve, demonstrating that birefringence-induced comb filtering effect plays an important role in dual-wavelength operation. In view that the birefringence-induced comb filter has multipeak transmission maxima, occasionally, three- or four- wavelength operation could be still observed by adjusting PCs as well. However, due to gain competition between the two neighboring peak-transmission wavelengths, the lasing wavelengths should be largely separated in order to suppress mutual gain competition. Together with the gain bandwidth limitation, it can explain why dual-wavelength Q-switching is more readily observed.

4. Conclusion

We demonstrate a wavelength-switchable, dual-wavelength synchronously Q-switched fiber laser based on graphene SA. The two lasing peaks are located at 1531.12 nm and 1556.79 nm with a wavelength spacing of 25.6 nm. The single pulse energy can reach up to $\sim$70 nJ. Wavelength resolved spectra show that pulse at each wavelength has the same repetition rate and they copropagate in the cavity. By rotating PCs in order to properly adjust the cavity birefringence, another state with dual-wavelength peaked at 1555.8 nm and 1561.5 nm and a wavelength spacing of 5.7 nm can be switched. These properties make our dual-wavelength Q-switched fiber laser suitable for optical clock synchronization.

References

[1] P. Urquhart, "Review of rare earth doped fibre lasers and amplifiers," *Proc. Inst. Elect. Eng. J—Optoelectron.*, vol. 135, no. 6, pp. 385–407, Dec. 1988.

[2] A. Kurkov, Y. Sadovnikova, A. Marakulin, and E. Sholokhov, "All fiber Er-Tm Q-switched laser," *Laser Phys. Lett.*, vol. 7, no. 11, pp. 795–797, Nov. 2010.

[3] Q. Lou, J. Zhou, B. He, and H. Zhou, "Fiber lasers and their coherent beam combination," *Opt. Photon. News*, vol. 19, no. 5, pp. 46–51, May 2008.

[4] U. Sharma, C. Kim, and J. Kang, "Highly stable tunable dual-wavelength Q-switched fiber laser for DIAL applications," *IEEE Photon. Technol. Lett.*, vol. 16, no. 5, pp. 1277–1279, May 2004.

[5] H. Shen, Y. Zhou, W. Lin, Z. Zeng, R. Zeng, G. Yu, C. Huang, A. Jiang, S. Jia, and D. Shen, "Second harmonic generation and sum frequency mixing of dual wavelength Nd:$YAlO_3$ laser in flux grown $KTiOPO_4$ crystal," *IEEE J. Quantum Electron.*, vol. 28, no. 1, pp. 48–51, Jan. 1992.

[6] H. Shen, W. Lin, R. Zeng, Y. Zhou, G. Yu, C. Huang, Z. Zeng, W. Zhang, R. Wu, and Q. Ye, "1079.5- and 1341.4-nm: Larger energy from a dual-wavelength Nd:$YAlO_3$ pulsed laser," *Appl. Opt.*, vol. 32, no. 30, pp. 5952–5957, Oct. 1993.

[7] H. Su, H. Shen, W. Lin, R. Zeng, C. Huang, and G. Zhang, "Computational model of Q-switch Nd:$YAlO_3$ dual-wavelength laser," *J. Appl. Phys.*, vol. 84, no. 12, pp. 6519–6522, Dec. 1998.

[8] A. Brenier, C. Tu, Z. Zhu, and B. Wu, "Red-green-blue generation from a lone dual-wavelength $GdAl_3(BO_3)_4 : Nd^{3+}$ laser," *Appl. Phys. Lett*, vol. 84, no. 12, pp. 2034–2036, Mar. 2004.

[9] S. Hu, J. Yu, C. Gao, G. Wei, and F. Lv, "Dual-wavelength stable nanosecond pulses generation from cladding-pumped fiber laser," *Chin. Opt. Lett.*, vol. 4, no. 11, pp. 655–657, Nov. 2006.

[10] L. Pan, I. Utkin, and R. Fedosejevs, "Two-wavelength passively Q-switched ytterbium doped fiber laser," *Opt. Exp.*, vol. 16, no. 16, pp. 11858–11870, Aug. 2008.

[11] A. Lagatsky, A. Abdolvand, and N. Kuleshov, "Passive Q-switching and self-frequency Raman conversion in a diode-pumped Yb:$KGd(WO_4)_2$ laser," *Opt. Lett.*, vol. 25, no. 9, pp. 616–618, May 2000.

[12] Y. Song, S. Jang, W. Han, and M. Bae, "Graphene mode-lockers for fiber lasers functioned with evanescent field interaction," *Appl. Phys. Lett.*, vol. 96, no. 5, pp. 051122–051124, Feb. 2010.

[13] Q. Bao, H. Zhang, Y. Wang, Z. Ni, Y. Yan, Z. Shen, K. Loh, and D. Tang, "Atomic-layer graphene as a saturable absorber for ultrafast pulsed lasers," *Adv. Funct. Mater.*, vol. 19, no. 19, pp. 3077–3083, Oct. 2009.

[14] H. Zhang, Q. Bao, D. Tang, L. Zhao, and K. Loh, "Large energy soliton erbium-doped fiber laser with a graphene-polymer composite mode locker," *Appl. Phys. Lett.*, vol. 95, no. 14, pp. 141103–141105, Oct. 2009.

[15] R. Newson, J. Dean, B. Schmidt, and H. van Driel, "Ultrafast carrier kinetics in exfoliated graphene and thin graphite films," *Opt. Exp.*, vol. 17, no. 4, pp. 2326–2333, Feb. 2009.

[16] D. Popa, Z. Sun, T. Hasan, F. Torrisi, F. Wang, and A. Ferrari, "Graphene Q-switched, tunable fiber laser," *Appl. Phys. Lett.*, vol. 98, no. 7, pp. 073106–073108, Feb. 2011.

[17] H. Zhang, D. Tang, L. Zhao, Q. Bao, K. Loh, B. Lin, and S. Tjin, "Compact graphene mode-locked wavelength-tunable erbium-doped fiber lasers: From all anomalous dispersion to all normal dispersion," *Laser Phys. Lett.*, vol. 7, no. 8, pp. 591–596, Aug. 2010.

[18] H. Zhang, D. Tang, R. Knize, L. Zhao, Q. Bao, and K. Loh, "Graphene mode locked, wavelength-tunable, dissipative soliton fiber laser," *Appl. Phys. Lett.*, vol. 96, no. 11, pp. 111112–111114, Mar. 2010.

[19] L. Zhao, D. Tang, H. Zhang, X. Wu, Q. Bao, and K. Loh, "Dissipative soliton operation of an ytterbium-doped fiber laser mode locked with atomic multilayer graphene," *Opt. Lett.*, vol. 35, no. 21, pp. 3622–3624, Nov. 2010.

[20] H. Zhang, D. Tang, L. Zhao, Q. Bao, and K. Loh, "Large energy mode locking of an erbium-doped fiber laser with atomic layer graphene," *Opt. Exp.*, vol. 17, no. 20, pp. 17630–17635, Sep. 2009.

[21] Z. Luo, M. Zhou, J. Weng, G. Huang, H. Xu, C. Ye, and Z. Cai, "Graphene-based passively Q-switched dual-wavelength erbium-doped fiber laser," *Opt. Lett.*, vol. 35, no. 21, pp. 3709–3711, Nov. 2010.

[22] S. Stankovich, D. Dikin, R. Piner, K. Kohlhaas, A. Kleinhammes, Y. Jia, Y. Wu, S. Nguyen, and R. Ruoff, "Synthesis of graphene-based nanosheets via chemical reduction of exfoliated graphite oxide," *Carbon*, vol. 45, no. 7, pp. 1558–1565, Mar. 2007.

[23] A. Martinez, K. Fuse, B. Xu, and S. Yamashita, "Optical deposition of graphene and carbon nanotubes in a fiber ferrule for passive mode-locked lasing," *Opt. Exp.*, vol. 18, no. 22, pp. 23054–23061, Oct. 2010.

[24] K. Kashiwagi, S. Yamashita, and S. Set, "In-situ monitoring of optical deposition of carbon nanotubes onto fiber end," *Opt. Exp.*, vol. 17, no. 7, pp. 5711–5715, Mar. 2009.

[25] Z. Sun, T. Hasan, F. Torrisi, D. Popa, G. Privitera, F. Wang, F. Bonaccorso, D. Basko, and A. Ferrari, "Graphene mode-locked ultrafast laser," *ACS Nano*, vol. 4, no. 2, pp. 803–810, Feb. 2010.

[26] S. Pan and C. Lou, "Stable multi-wavelength dispersion-tuned actively mode-locked erbium-doped fiber ring laser using nonlinear polarization rotation," *IEEE Photon. Technol. Lett.*, vol. 18, no. 13, pp. 1451–1453, Jul. 2006.

[27] Z. Luo, A. Luo, W. Xu, H. Yin, J. Liu, Q. Ye, and Z. Fang, "Tunable multiwavelength passively mode-locked fiber ring laser using intracavity birefringence-induced comb filter," *IEEE Photon. J.*, vol. 2, no. 4, pp. 571–577, Aug. 2010.

[28] C. Song, W. Xu, Z. Luo, A. Luo, and W. Chen, "Switchable and tunable dual-wavelength ultrashort pulse generation in a passively mode-locked erbium-doped fiber ring laser," *Opt. Commun.*, vol. 282, no. 22, pp. 4408–4412, Nov. 2009.

[29] A. Luo, Z. Luo, W. Xu, V. Dvoyrin, V. Mashinsky, and E. Dianov, "Tunable and switchable dual-wavelength passively mode-locked Bi-doped all-fiber ring laser based on nonlinear polarization rotation," *Laser Phys. Lett.*, vol. 8, no. 8, pp. 601–605, Aug. 2011.

[30] W. Man, H. Tam, M. Demokan, P. Wai, and D. Tang, "Mechanism of intrinsic wavelength tuning and sideband asymmetry in a passively mode-locked soliton fiber ring laser," *J. Opt. Soc. Am. B*, vol. 17, no. 1, pp. 28–33, Jan. 2000.

[31] D. Tang, L. Zhao, B. Zhao, and A. Liu, "Mechanism of multisoliton formation and soliton energy quantization in passively mode-locked fiber lasers," *Phys. Rev. A*, vol. 72, no. 4, pp. 043816–043824, Oct. 2005.

[32] H. Xu, D. Lei, S. Wen, X. Fu, J. Zhang, Y. Shao, L. Zhang, H. Zhang, and D. Fan, "Observation of central wavelength dynamics in erbium-doped fiber ring laser," *Opt. Exp.*, vol. 16, no. 10, pp. 7169–7174, May 2008.